Supporting Information

Synthesis, Characterisation and Thermal Behaviour of Solid Phases in the Quasi-Ternary System $Mg(SCN)_2$ - H_2O - THF

Markus Joos[a], Maurice Conrad[b], Rotraut Merkle[a], Thomas Schleid[b], Joachim Maier[a], Robert E. Dinnebier[a] and Sebastian Bette*[b]

*E-Mail: S.Bette@fkf.mpg.de

Experimental

General

After synthesis, the powder samples were prepared, handled, and measured under dry inert gas (Ar or N_2 with < 1 ppm H_2O) or vacuum unless stated otherwise. The samples were stored in small screw cap vials under argon in a glove box. Some transfer steps required exposing the samples to air for a short time, on the order of minutes. Both $Mg(SCN)_2 \cdot 4\ H_2O$ and $Mg(SCN)_2 \cdot 4$ THF were stable under inert gas conditions without any detectable loss of H_2O or THF, however, $Mg(SCN)_2 \cdot 2\ H_2O \cdot 2$ THF appeared to decompose even when stored under argon.

Synthesis

$Mg(SCN)_2 \cdot 4\ H_2O$

Two different synthesis strategies were employed for $Mg(SCN)_2 \cdot 4\ H_2O$. In the first one $MgCl_2 \cdot 6\ H_2O$ (99.995 % *Aldrich*; 99.999 % *Alfa Aesar*) was dissolved in dry ethanol (≥99.8 % *Roth*, ≤2000 ppm H_2O) and while stirring KSCN (≥99.0 % *Sigma-Aldrich*) was added gradually in the respective stoichiometric amount (for 1 g of $MgCl_2 \cdot 6\ H_2O$ about 50 ml of ethanol were used).[1] Afterwards KCl started to precipitate and the solution was left stirring for ~0.5-2 h (the precipitate was confirmed to be KCl by XRPD). The precipitated KCl was consequently filtered off (either by vacuum filtering or without suction) and the ethanol was mostly removed by vacuum distillation with a standard laboratory rotary evaporator set-up (*BÜCHI*, Rotavapor R-114, Waterbath B-480, *vacuubrand* membrane vacuum pump). The resulting viscous slurry was mixed with ~50 ml deionized H_2O and then stirred for ~0.5-1 h. Afterwards most of the H_2O was removed at the rotary evaporator and the final product was precipitated by freeze drying (Freeze Dryer *Scientz*-10N, China). The precipitate consisted of white, transparent crystallites, which were confirmed to be phase pure $Mg(SCN)_2 \cdot 4\ H_2O$ (with ~2 wt.-% KCl contamination) by XRPD.
An alternative synthesis route was to employ a cation-exchange column filled with hydrogen-form Amberlite® IR-120 (*Fluka*, Switzerland), which was loaded with Mg^{2+} cations by passing through an aqueous solution of $MgCl_2 \cdot 6\ H_2O$ (400 g in 1800 mL, 99 % *Grüssing*). After washing the column with deionized water, an aqueous solution of KSCN (4.5 g in 150 mL deionized water, p.a. *Merck*) was passed through and subsequently most of the water was removed under reduced pressure in a rotary evaporator. Finally, the residual solution was transferred into a desiccator and dried over silica gel yielding 4.85 g (97 % theoretical yield) of phase pure $Mg(SCN)_2 \cdot 4\ H_2O$ as colourless, transparent and hygroscopic platelets.

$Mg(SCN)_2 \cdot 2\ H_2O \cdot 2$ THF

The synthesis of $Mg(SCN)_2 \cdot 2\ H_2O \cdot 2$ THF was similar to the one of the tetrahydrate described above ($MgCl_2 \cdot 6\ H_2O$ with KSCN in ethanol). However, after removing most of the ethanol by vacuum distillation with a rotary evaporator, about 50 ml of tetrahydrofuran (THF, ROTIDRY ≥99.9 % *Roth*; anhydrous ≥99.9 % inhibitor free, *Sigma-Aldrich*) were added to the slurry instead of deionized H_2O. The solution was again stirred for ~0.5-1 h and most of the THF was finally removed with the rotary evaporator. Afterwards, the flask containing the concentrated solution was put into a sand bath, connected to a Schlenk line and the remaining THF was removed at 30 °C under higher vacuum (~10^{-2} mbar). After approximately 4 h white, transparent crystallites started to precipitate slowly and the THF evaporation was continued to full dryness. Finally, the flask was disconnected from the Schlenk line and transferred into an Ar filled glove box. The final product was confirmed to be phase pure $Mg(SCN)_2 \cdot 2\ H_2O \cdot 2$ THF (with ~2 wt.-% KCl contamination) by XRPD. We would like to mention that the synthesis described here did not always

produce phase pure $Mg(SCN)_2 \cdot 2\ H_2O \cdot 2$ THF and we encountered significant experimental difficulty in synthesizing as well as preserving this phase.

$Mg(SCN)_2 \cdot 4$ THF

As was already described for the synthesis of $Mg(SCN)_2 \cdot 2\ H_2O \cdot 2$ THF, $MgCl_2 \cdot 6\ H_2O$ and KSCN were dissolved in ethanol, the ethanol was mostly removed and about 50 ml of THF were added (see above for more details). Yet in contrast, all THF was removed by vacuum distillation directly at the rotary evaporator until a yellow powder precipitated, which was later determined to be a mixture of $Mg(SCN)_2 \cdot 2\ H_2O \cdot 2$ THF and $Mg(SCN)_2 \cdot 4$ THF. To isolate the THF-rich phase, the powder was transferred into an Ar filled glove box, and under argon atmosphere redissolved in ~80 ml of dry THF (anhydrous ≥99.9 % inhibitor free, *Sigma-Aldrich*). The mixture was left stirring for ~12 h, yet the powder did not fully dissolve in THF. In order to remove the remaining H_2O, a three-neck flask containing the THF mixture was connected to a Schlenk line under Ar atmosphere, adapted with a Dimroth condenser, and the mixture was refluxed for ~20 minutes at 90 °C, while flushing the set-up with argon. After cooling to room temperature, the THF was directly removed at the Schlenk line by vacuum distillation and the flask was then transferred into a glove box. The precipitate was again a yellow powder, which was later confirmed to be phase pure $Mg(SCN)_2 \cdot 4$ THF (with ~2 wt.-% KCl contamination) by XRPD.

Phase Characterization

The X-ray powder diffraction (XRPD) patterns for structure determinations were collected at room temperature on a laboratory powder diffractometer in Debye-Scherrer geometry (Stadi P-diffractometer (Stoe), Cu-$K_{\alpha1}$ radiation from primary Ge(111)-Johannson-type monochromator, triple array of Mythen 1 K detectors (Dectris)). The samples were sealed in either 0.5 or 0.7 mm borosilicate glass capillaries (Hilgenberg glass no. 14), which were spun during the measurements. Patterns for structure determinations were measured in a 2θ range from 5.0° to 110.0° applying a total scan time of 4 h.

Additionally, XRPD patterns for phase confirmations and decomposition products were recorded in a Bragg-Brentano configuration at room temperature (PANalytical Empyrean Series 2 diffractometer, Cu-$K_{\alpha1}$, 40 kV, 40 mA, PIXcel 3D detector, 2θ = 10°-90°) and analyzed with the PANalytical HighScore Plus software (Version 3.0e). The samples were measured either at air or in a polycarbonate dome (PANalytical) under Ar atmosphere.

The crystal structures of $Mg(SCN)_2 \cdot 2\ H_2O \cdot 2$ THF, α-$Mg(SCN)_2 \cdot 4$ THF, β-$Mg(SCN)_2 \cdot 4$ THF and $Mg(SCN)_2 \cdot 2$ THF were determined *ab initio* from the XRPD data by using the program TOPAS 6.0,[2] the crystal structure of $Mg(SCN)_2 \cdot 4\ H_2O$ was Rietveld refined using the crystal structure published by Mereiter et al. as starting model.[3,4]

Temperature dependent *in situ* XRPD measurements

Temperature dependent *in situ* XRPD experiments on $Mg(SCN)_2 \cdot 4\ H_2O$ were performed using the device and sample preparation described above. A hot and cool air blower (Cobra 700, Oxford Cryosystems) was used to cool down the sample to -100 °C and to heat it up to 220 °C. The heating was performed in 10 K steps using a heating rate of 5 K/min and an equilibration time of 5 minutes. XRPD pattern were recorded subsequently in a 2θ range from 0.0° to 110.0° applying a total scan time of 30 minutes.

Temperature dependent *in situ* XRD experiments on $Mg(SCN)_2 \cdot 4$ THF were performed on a D8-Advance diffractometer (Bruker, Cu-$K_{\alpha1}$ radiation from primary Ge(111)-Johannson-type monochromator, Lynx Eye position sensitive detector (Bruker)) in Debye-Scherrer geometry using a water cooled furnace (mri capillary heater, 25-1000 °C) for heating the capillary. The samples were prepared with the same procedure as described above. In a first run, the thermal behavior was monitored. Therefore, XRPD patterns were collected in a 2θ range from 5.0° to 40.0° applying a total scan time of 2 h. From 30 °C to 100 °C, the sample was heated in 5 K steps with a heating rate of 10 K/min, from 100 °C to 260 °C in 10 K steps and from 260 °C to 300 °C in 20 K steps. Prior to each measurement a delay time of 10 minutes was applied in order to ensure thermal equilibration. For detailed structural analyses on the thermal decomposition products, XRPD patterns were collected in a 2θ range from 8.0° to 90.0° applying a total scan time of 12 h. The sample was heated up to 130 °C with a heating rate of 2 K/min and a subsequent isothermal phase of 2 h. Afterwards the sample was heated up to 240 °C in 5 K steps with a heating rate of 10 K/min. At each step, one XRPD pattern was collect with a preceding delay time of 15 minutes in order to ensure thermal equilibration.

The refined crystal structures of $Mg(SCN)_2 \cdot 4\ H_2O$, α-$Mg(SCN)_2 \cdot 4$ THF, β- $Mg(SCN)_2 \cdot 4$ THF and $Mg(SCN)_2 \cdot 2$ THF were used for Rietveld refinements of the *in situ* XRPD patterns,[3] in order to analyze the temperature dependent evolution of the lattice parameters and the unit cell volumes. Within a series of *in situ* XRPD patterns, all refinements were carried out by a sequential approach as previously described.[5] The volume thermal expansion coefficients and all axes expansion coefficients were calculated from the refined lattice parameters by using the PASCal software.[6]

Infrared Spectroscopy (IR)

Infrared (IR) spectroscopy was performed both in air and under Ar atmosphere inside a glove box. In air, the measurements were performed on a Spectrum Two spectrometer (Perkin Elmer) with a universal attenuated total reflection (UATR) unit, for which the data was collected with the software Spectrum 10. Measurements under Ar were performed on an ALPHA II FT-IR (Fourier-transform) spectrometer from Bruker Optik GmbH, also with an ATR unit. Measurement data were collected with the software OPUS from Bruker.

Thermogravimetric Analysis (TGA)

About 30-40 mg of sample powder were transferred into a TGA set-up inside a quartz crucible. The samples were exposed to atmosphere for approximately 30 seconds during the transfer. Measurements were conducted on a Netzsch STA 449 instrument with a protective N_2 gas flow (< 10 ppm H_2O including trace leaks, 60 ml/min). The samples were first heated to 200 °C for ~0.5 h and afterwards further heated to 400 °C for ~1 h (heating rate: 2 K/min). The exhaust gas of the TGA experiments was analyzed by a Balzers Prisma quadrupole mass spectrometer (MS). Buoyancy correction was omitted, since the recorded sample mass changes rendered buoyancy effects negligible.

Differential Scanning Calorimetry (DSC)

Differential scanning calorimetry (DSC) was conducted on a DSC 214 *Polyma* (Netzsch). The sample was weighed in an aluminum pan, fitted with an aluminum lid and finally cold welded under Ar. The cold welded seal was gas tight at room temperature, however, at elevated temperatures the loss of H_2O or THF could not be fully avoided (semi-closed system). For each sample, at least two temperature cycles were performed (heating and cooling rate: 5 K/min). Inside the DSC, the crucible was constantly flushed with 40 ml/min protective and 60 ml/min purging N_2 gas. A cold welded and pierced empty Al pan was used as reference.

Scanning Electron Microscopy (SEM) and Energy Dispersive X-Ray (EDX) Analysis

SEM images were collected both on a Vega TS 5130 MM (Tescan) and a Merlin (Zeiss) microscope, and EDX measurements were conducted with the detector Ultim® Extreme (Oxford Instruments) Prior to imaging, samples were placed on carbon tape and coated either with gold or carbon. The transfer steps were performed with very short exposure to air or completely under inert conditions (high vacuum or inert gas).

Crystal Structure Refinement and Determination

The program TOPAS 6.0 was used to determine and refine the crystal structures of $Mg(SCN)_2 \cdot (4\text{-}x)\ H_2O \cdot x\ THF$ (x = 0, 2, 4) (Figure S1) with additional information from IR measurements (Figure S3) and SEM-EDX (Figure S4 and Figure S5).[2] Indexing of the phases was carried out by an iterative use of singular value decompositions (LSI).[7] The peak profile and the precise lattice parameters were determined by LeBail applying the fundamental parameter approach of TOPAS.[8–10] The background was modelled by employing Chebychev polynomials of 6th order, the refinement converged quickly. During the refinement the presence of additional peaks attributed to KCl was observed. Hence the crystal structure of KCl was included into the refinement and into the subsequent process of crystal structure determination.[11] Selected bond lengths and angles for all compounds are given in Table S3, Table S6 and Table S9 and all crystallographic data sets were deposited in the CCDC database under the depositions numbers: 2055308-2055312.

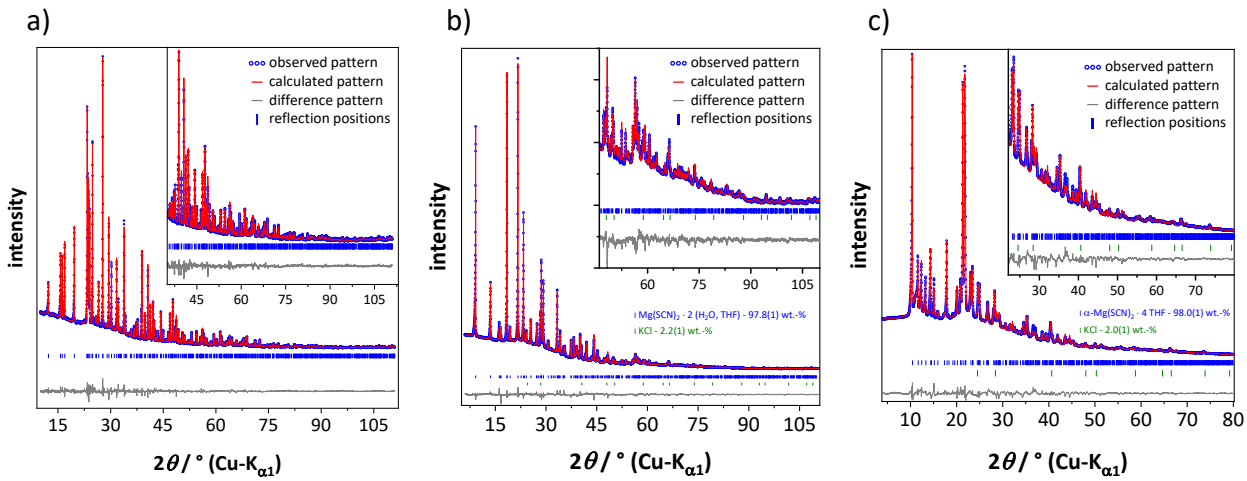

Figure S1: Rietveld refinement plots of XRPD patterns in the series $Mg(SCN)_2 \cdot (4\text{-}x)\ H_2O \cdot x$ THF of the phases; a) $x = 0$; b) $x = 2$; c) $x = 4$.

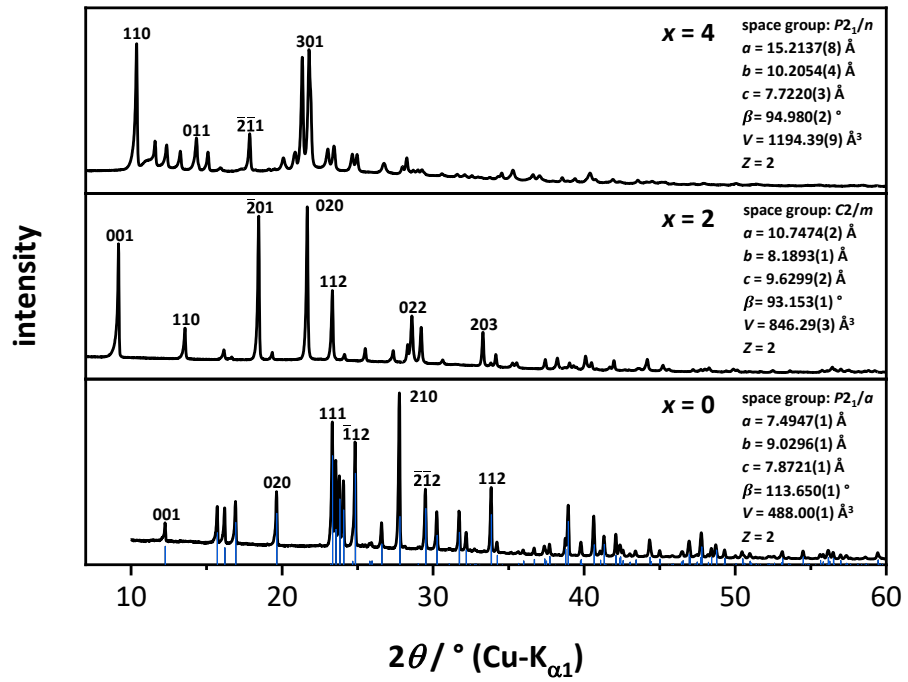

Figure S2: Indexed XRPD patterns of $Mg(SCN)_2 \cdot (4\text{-}x)\ H_2O \cdot x$ THF phases with $x = 0$, 2 and 4. The blue lines correspond to the calculated reflection positions from the reported crystal structure of $Mg(SCN)_2 \cdot 4\ H_2O$.[4]

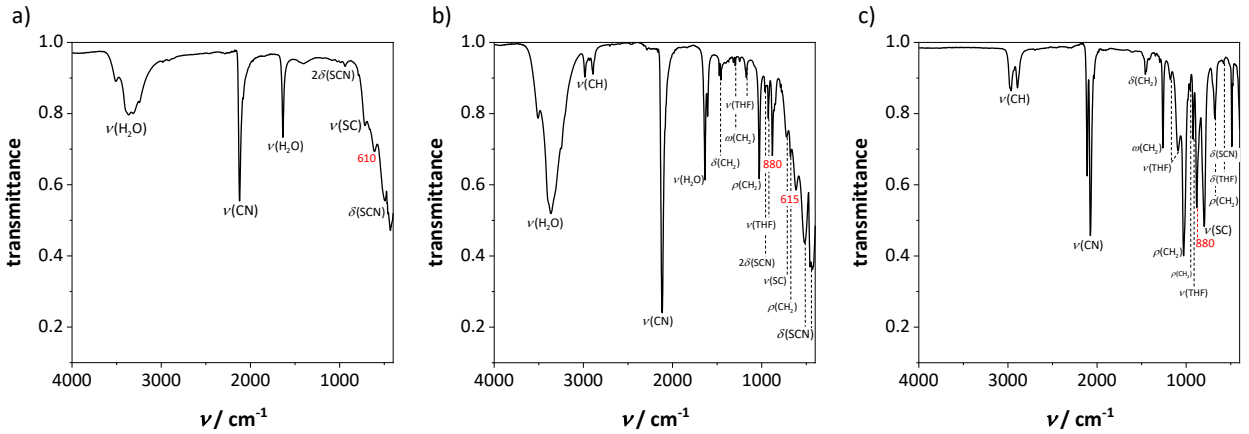

Figure S3: IR spectra of $Mg(SCN)_2 \cdot (4\text{-}x)\ H_2O \cdot x$ THF phases with; a) $x = 0$ (measured in Ar); b) $x = 2$ (measured in air); c) $x = 4$ (measured in Ar).

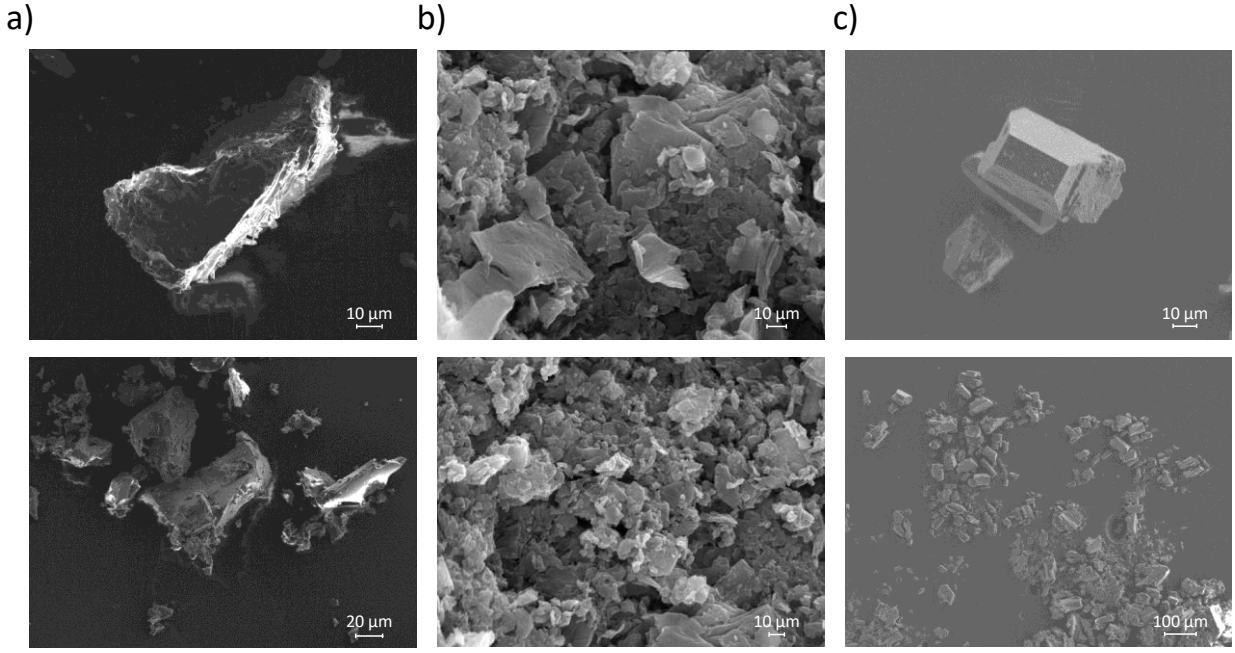

Figure S4: SEM images of $Mg(SCN)_2 \cdot (4\text{-}x)\ H_2O \cdot x$ THF phases; a) $x = 0$; b) $x = 2$; c) $x = 4$.

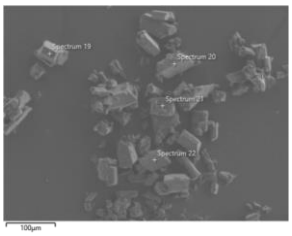

atom	Spectrum 19		Spectrum 20		Spectrum 21		Spectrum 22		average	
	at.-%	at.-% sigma	at.-%	at.-% sigma	at.-%	at.-% sigma	at.-%	at.-% sigma	at.-%	at.-% sigma
N	3.7	0.2	8.4	0.3	18.5	0.4	12.6	0.3	10.8	0.3
O	22.7	0.3	15.9	0.2	68.3	0.5	28.7	0.3	33.9	0.3
Mg	17.5	0.2	11.3	0.1	3.6	0.2	17.7	0.2	12.5	0.2
Si	27.8	0.2	36.9	0.2	9.3	0.2	23.8	0.2	24.5	0.2
S	28.3	0.3	27.5	0.2	0.4	0.2	17.2	0.2	18.4	0.2

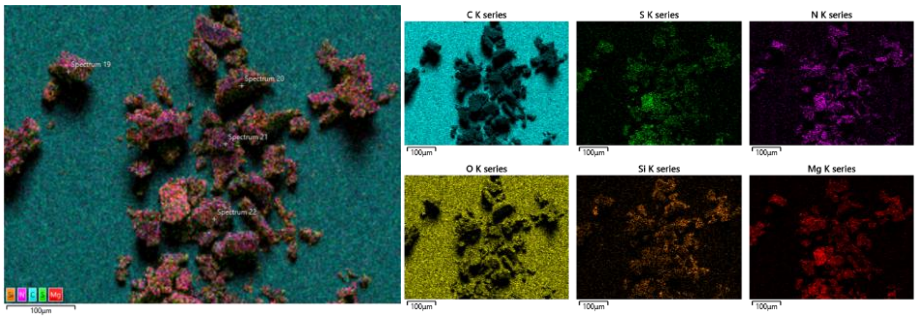

atom	Map	
	at.-%	at.-% sigma
N	6.5	0.1
O	71.5	0.2
Mg	5.32	0.07
Si	7.61	0.09
S	7.9	0.1
Na	1.16	0.06

Figure S5: EDX results of $Mg(SCN)_2 \cdot 4$ THF either by measuring individual grains (upper half) or by creating an elemental map (lower half). The rather high amount of Si can be attributed to the used silicone-based vacuum grease that was employed in several synthesis and preparation steps.

$Mg(SCN)_2 \cdot 4\ H_2O$

An attempt to fit the XRPD pattern of $Mg(SCN)_2 \cdot 4\ H_2O$ using the crystal structure published by Mereiter et al.,[4] which was obtained by single crystal X-ray diffraction, did not lead to a satisfying result (Figure S6a, R-wp = 4.52 %). Hence, the structural model of $Mg(SCN)_2 \cdot 4\ H_2O$ derived from single crystal diffraction does not seem to be entirely representative for the microcrystalline bulk material. Accordingly, the program TOPAS 6.0[2] was used to refine the crystal structure of $Mg(SCN)_2 \cdot 4\ H_2O$ by using the structural data of Mereiter et al.[4] as a starting model. The method of simulated annealing (SA) in real space as implemented in TOPAS[12] was applied for global optimization of the powder pattern. The thiocyanate related C, N and S sites were constrained by a rigid body set up in z-matrix notation. The rigid body and two water related oxygen sites were moved freely throughout the unit cell, the magnesium site did not have any translational degree of freedom, as it is located on a symmetry centre. In the Rietveld refinement,[3] all profile and lattice parameters were released iteratively, the lengths and angles of the rigid bodies were refined, restraining them to reasonable values and the hydrogen positions were omitted due to the limits of the powder diffraction method. This led to a substantial improvement of both in the R-wp value (R-wp = 3.32) and in the graphical result of the refinement (Figure S6b). The crystallographic data are given in Table S1-Table S3.

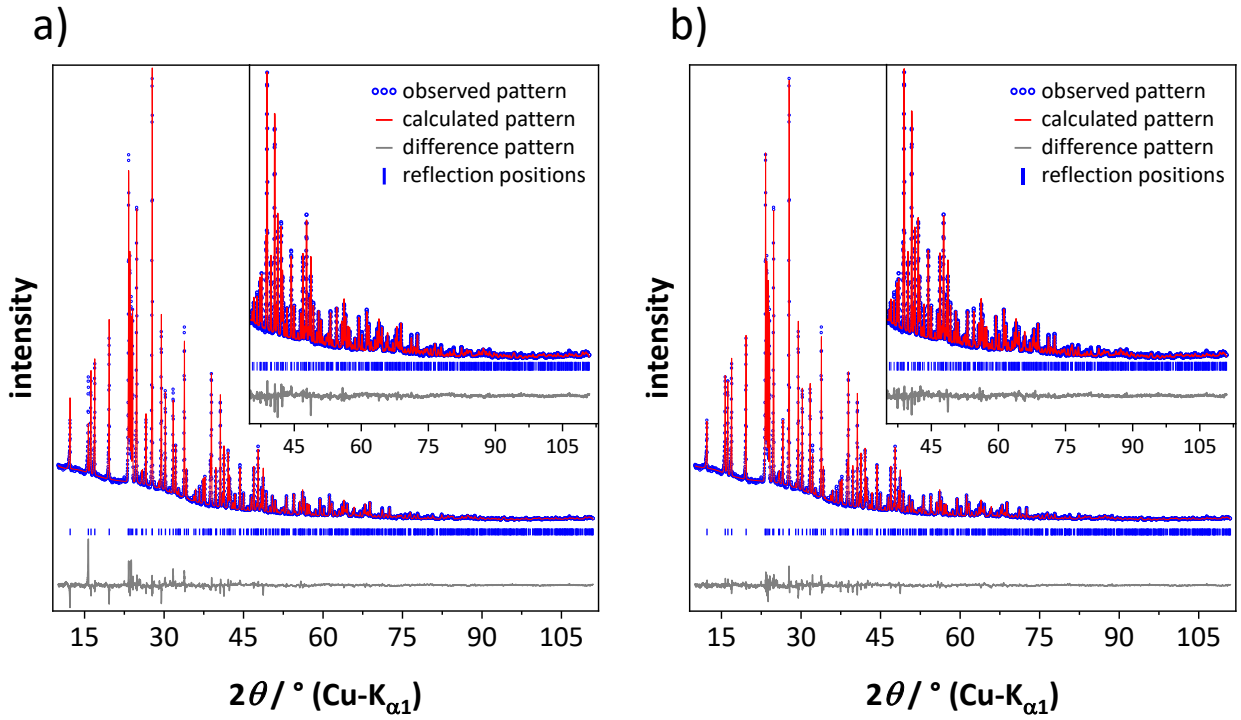

Figure S6: Final Rietveld refinement plots of the crystal structure of $Mg(SCN)_2 \cdot 4\ H_2O$; a) using the structural model by Mereiter et al.[4] obtained by single crystal X-ray diffraction (R-wp = 4.52 %); b) by global optimization of the XRPD pattern (R-wp = 3.32 %), the region above 35° 2θ is enlarged for clarity (inserts).

Table S1: Crystallographic and Rietveld refinement data of $Mg(SCN)_2 \cdot 4\ H_2O$.

compound name	magnesium thiocyanate tetrahydrate
molecular formula	$Mg(SCN)_2 \cdot 4\ H_2O$
sum formula	$C_2H_8MgN_2O_4S_2$
molecular weight/ g/mol	244.537
temperature/ K	298
space group	$P2_1/a$ (no. 14)
Z	2
a /Å	7.4947(1)
b /Å	9.0296(1)
c /Å	7.8721(1)
β /°	113.650(1)
V /Å³	488.00(1)
ρ_{calc}/ g · cm^{-3}	1.45
wavelength / Å	1.5406
R-p /% [a)]	2.52
R-wp /% [a)]	3.32
R-F^2 /% [a)]	1.98
no. of variables	45

[a)] R-exp, R-p, R-wp and R-F^2 as defined in TOPAS (Bruker AXS).

Table S2: Atomic coordinates of $Mg(SCN)_2 \cdot 4\ H_2O$.

Atom	Wyck.	Site	S.O.F.	x	y	z	B / Å²
Mg(1)	2a	-1	1	0	0	0	3.0(1)[a)]
O(1)	4e	1	1	0.0634(3)	0.1096(2)	0.7860(3)	3.0(1)[a)]
O(2)	4e	1	1	0.2793(3)	0.9130(2)	0.1068(3)	3.0(1)[a)]
S(11)	4e	1	1	0.8183(6)	0.5658(5)	0.5969(6)	3.0(1)[a)]
C(11)	4e	1	1	0.8643(5)	0.7123(4)	0.7314(5)	3.0(1)[a)]
N(11)	4e	1	1	0.8966(5)	0.8152(3)	0.8259(4)	3.0(1)[a)]

[a)] one global parameter for the Beq of all sites was defined.

Table S3: Selected bond distances and angles in $Mg(SCN)_2 \cdot 4\ H_2O$.

Atoms	Distance / Å	Atoms	Angle / °
Mg(1)-O(1)	2x 2.164(2)	O(1)-Mg(1)-O(2)	89.3(1), 90.7(1)
Mg(1)-O(2)	2x 2.072(2)	O(1)-Mg(1)-N(11)	89.7(1), 90.3(1)
Mg(1)-N(11)	2x 2.101(2)	O(2)-Mg(1)-N(11)	89.3(1), 90.7 (1)

$Mg(SCN)_2 \cdot 2\ H_2O \cdot 2$ THF

In a first attempt to solve the crystal structure of $Mg(SCN)_2 \cdot 2\ H_2O \cdot 2$ THF the global optimization method of simulated annealing (SA) in real space as implemented in TOPAS was applied,[12] originally assuming a phase composition of $Mg(SCN)_2$. According to the estimated cell volume (Table S4) and to the packing density of $Ni(SCN)_2$,[13] as a probable related phase, a content of 8 formula units per unit cell was assumed. Different sets of Mg^{2+} and SCN^- ions, the latter ones defined in z-matrix notation, were placed into the unit cell and moved and rotated freely within the cell. Atoms located on identical positions and occupying special positions were identified by using a merging radius of 0.7 Å.[14] After numerous attempts, however, the process did not lead to a reasonable structure model. Neither the decrease of the starting set of ions from 8 to 6 formula units or a symmetry reduction of the unit cell or the introduction of a triclinic distortion of the unit cell led to a successful structure solution. The method of Charge Flipping with histogram matching supported by inclusion of the tangent formula was used as an alternative approach to solve the crystal structure.[15–17] For the first run using space group *C2/m* with 8 formula units (8 Mg^{2+} cations and 16 C, S and N atoms) were included into the Charge Flipping process. In the resulting structural model linear units, octahedra and fivefold rings were present. As IR spectroscopy (Figure S3) indicated the presence of both water and THF either as adherent solvent or as components of the solid, the linear units were assigned to SCN^- anions, the fivefold rings to THF (C_4H_8O) molecules and the octahedra to $Mg(NCS)_2(H_2O)_2(THF)_2$ units. Accordingly, a second run of Charge Flipping was performed with a starting set of 2 Mg^{2+} cations, 20 C, 4 N, 4 S and 8 O atoms referring to two formula units of $Mg(SCN)_2 \cdot 2\ H_2O \cdot 2$ THF. After a few minutes, an adequate structural model was obtained. The SCN^- anion and the THF molecule were constraint as rigid bodies defined in z-matrix notation. According to the structural model obtained by Charge Flipping, both the thiocyanate anion and the THF molecule are situated on the mirror plane. Due to the non-planar conformation of THF, either the molecule is disordered, or it breaks the *C2/m* symmetry and reduces the space group symmetry to *C2*. In a first attempt, the crystal structure was refined using the centrosymmetric space group *C2/m*. The THF related oxygen atoms were placed on the mirror plane and the occupancies of the carbon atoms were set to 0.5 (Figure 7b). Symmetry adapted spherical harmonics of 4th order were applied in order to account for anisotropic peak broadening caused by further disorder of the THF molecules. In the final Rietveld refinement,[3] all profile and lattice parameters were released iteratively. The lengths and angles of the rigid bodies were refined while restraining them to reasonable values and the hydrogen positions were omitted due to the limits of the powder diffraction method. This led to a reasonable structural model with good agreement factors (Table S4) and a satisfying agreement between the measured and calculated powder pattern (Figure S1b). In a second attempt, the refined structure was used as a starting model for a Rietveld refinement using the non-centrosymmetric space group *C*2. Due to the absence of the mirror plane this model did not describe any disorder of the THF molecule. The final Rietveld refinement led to a worse fit of the powder pattern. Residual electron density in the proximity of the THF related carbon sites, which was observed by inspection of the difference Fourier map, indicated a positional disorder of the THF molecule. Accordingly, a second THF molecule was introduced and the oxygen atoms of both molecules were fixed at the same position. This led to an improvement of the fit. However, the structure could not be refined freely and the positions of the magnesium atoms had to be fixed and pseudo-centrosymmetric constraints had to be applied to the water related oxygen sites. The resulting fit was still worse than the one using space group *C*2/*m*. Hence, the structural model obtained for the centrosymmetric space group *C*2/*m* was evaluated as the best representative for the crystal structure of $Mg(SCN)_2 \cdot 2\ H_2O \cdot 2$ THF.

Table S4: Crystallographic and Rietveld refinement data of $Mg(SCN)_2 \cdot 2\ H_2O \cdot 2$ THF.

compound name	$Mg(SCN)_2 \cdot 2\ (H_2O, THF)$
molecular formula	$2(C_4H_8O)\cdot Mg(SCN)_2\cdot 2H_2O$
sum formula	$C_{10}H_{20}MgN_2O_4S_2$
molecular weight/ g/mol	320.715
temperature/ K	298
space group	*C*2/*m* (no. 12)
Z	2
a /Å	10.7474(2)
b /Å	8.1893(1)
c /Å	9.6299(2)
β /°	93.153(1)
V /Å³	846.29(3)
ρ_{calc}/ g · cm^{-3}	1.26
wavelength / Å	1.5406
R-p /% [a)]	1.81
R-*w*p /% [a)]	2.74
R-*F*² /% [a)]	1.85
no. of variables	53

[a)]R-exp, R-p, R-wp and R-F² as defined in TOPAS (Bruker AXS).

Table S5: Atomic coordinates of $Mg(SCN)_2 \cdot 2\ H_2O \cdot 2$ THF.

Atom	Wyck.	Site	S.O.F.	x	y	z	B / Å²
Mg(1)	2b	2/*m*	1	0	1/2	0	2.2(2)
O(1)	4g	2	1	0		0	3.0(2)
C(1)	4i	m	1	0.243(1)	0	0.170(1)	3.0(2)[a)]
N(1)	4i	m	1	0.338(1)	0	0.120(1)	3.0(2)[a)]
S(1)	4i	m	1	0.108(2)	0	0.242(1)	3.0(2)[a)]
O(11)	4i	m	1	0.881(1)	1/2	0.810(1)	2.1(2)[a)]
C(11)	8j	1	0.5	0.747(1)	0.463(2)	0.791(2)	2.1(2)[a)]
C(12)	8j	1	0.5	0.932(2)	0.511(1)	0.672(2)	2.1(2)[a)]
C(13)	8j	1	0.5	0.823(3)	0.517(4)	0.569(2)	2.1(2)[a)]
C(14)	8j	1	0.5	0.722(2)	0.433(4)	0.639(2)	2.1(2)[a)]

[a)]one global parameter for the Beq of the NCS^- and the THF related sites was defined.

Table S6: Selected bond distances and angles in $Mg(SCN)_2 \cdot 2\ H_2O \cdot 2$ THF.

Atoms	Distance / Å	Atoms	Angle / °
Mg(1)-O(1)	2x 1.993(4)	O(1)-Mg(1)-O(11)	2x 90
Mg(1)-O(11)	2x 2.176(5)	O(1)-Mg(1)-N(1)	2x 90
Mg(1)-N(1)	2x 2.136(5)	O(11)-Mg(1)-N(1)	89.7(2), 90.3(2)

$Mg(SCN)_2 \cdot 4$ THF

The crystal structure of α-$Mg(SCN)_2 \cdot 4$ THF was solved by applying the global optimization method of simulated annealing (SA) in real space as implemented in TOPAS.[12] The exact phase composition was unknown prior to the crystal structure solution. The unit cell volume (Table S7) and the space group symmetry pointed either to a phase composition of $Mg(SCN)_2 \cdot 2$ THF with 4 formula units per unit cell or to $Mg(SCN)_2 \cdot 4$ THF with 2 formula units per unit cell. The global optimization was carried out multiple times using different sets of magnesium and thiocyanate ions and THF molecules. The latter two were described by rigid bodies in z-matrix notation and rotated and translated freely through the unit cell. Atoms situated on identical or special positions were identified by using a merging radius of 0.7 Å.[14] All attempts led to a structural model that corresponds to a phase composition of $Mg(SCN)_2 \cdot 4$ THF with two formula units per unit cell and the magnesium cations situated on centres of inversion. The Rietveld refinement was conducted in the same manner as described above for $Mg(SCN)_2 \cdot 2\ H_2O \cdot 2$ THF.[3] A broad reflection at 11.2 ° 2θ and a broad hump in the background in the 2θ range between 20 ° and 26 ° indicated the presence of an amorphous by-product. Broad Lorentzian-type peaks were used to model the amorphous phase. An inspection of the difference Fourier map revealed some residual electron density close to one of the THF molecules and therefore indicated positional disorder. In order to partially compensate this a third THF molecule was introduced and its oxygen site constrained to the oxygen site (O(21), Table S8) of the second THF molecule (Figure 9a). Symmetry adapted spherical harmonics of 4th order were applied in order to account for anisotropic peak broadening caused by further disorder of the THF molecules. The final Rietveld refinement led to reasonable agreement factors (Table S7) and a good graphical result of the fit (Figure S1c).

Indexing of the XRPD pattern of the first decomposition product of α-$Mg(SCN)_2 \cdot 4$ THF led to a primitive monoclinic unit cell with space group $P2_1/a$. As the unit cell metric and volume (Table S7) was close to α-$Mg(SCN)_2 \cdot 4$ THF, we concluded that the first decomposition product is an additional polymorph of α-$Mg(SCN)_2 \cdot 4$ THF: β-$Mg(SCN)_2 \cdot 4$ THF. The crystal structure solution and refinement was carried out analogous to the procedure described for α-$Mg(SCN)_2 \cdot 4$ THF. A positional disorder of both crystallographically independent THF molecules could be observed (Figure 9b). The atomic coordinates of β-$Mg(SCN)_2 \cdot 4$ THF are given in Table S8 and the graphical result of the final Rietveld refinement in Figure S7b.

The XRPD pattern of the second thermal decomposition product of α-$Mg(SCN)_2 \cdot 4$ THF could be indexed with a *C*-cantered monoclinic unit cell and *C*2, *Cm* and *C*2/*m* as most possible space groups. From the unit cell volume, the space group symmetry and the thermal analysis (Figure 4) a phase composition of $Mg(SCN)_2 \cdot 2$ THF was estimated. All lattice parameters (Table S7) were observed to be very close to the unit cell of $Ni(SCN)_2$ except for the b-axis,[13] which was found to be considerably larger in the second thermal decomposition product of α-$Mg(SCN)_2 \cdot 4$ THF. Hence, a comparable, layered crystal structure with the layers broadened in *b*-direction by the THF molecules was expected. The crystal structure was finally solved by applying the global optimization method of simulated annealing (SA) using space group *C*2/*m* and the expected phase composition of $Mg(SCN)_2 \cdot 2$ THF could be confirmed. The magnesium cation could be located on an inversion centre, the THF related oxygen on a twofold symmetry axis and the thiocyanate related nitrogen on a mirror plane (Table S8). The entire thiocyanate anion is not situated on the mirror plane. Instead, the carbon and the sulphur atoms are positionally disordered (Figure 9c, magenta and violet atoms). The THF molecule was found to exhibit a fourfold positional disorder (Figure 9c, red, blue, yellow and green atoms). Any attempt to refine a more ordered structural model using space group *C*2 or *Cm* led to considerably worse results of the refinements. Hence, the disordered structural model using space group *C*2/*m* was evaluated as most suitable for $Mg(SCN)_2 \cdot 2$ THF at 443 K (170 °C). The graphical result of the final Rietveld refinement is shown in Figure S7c.

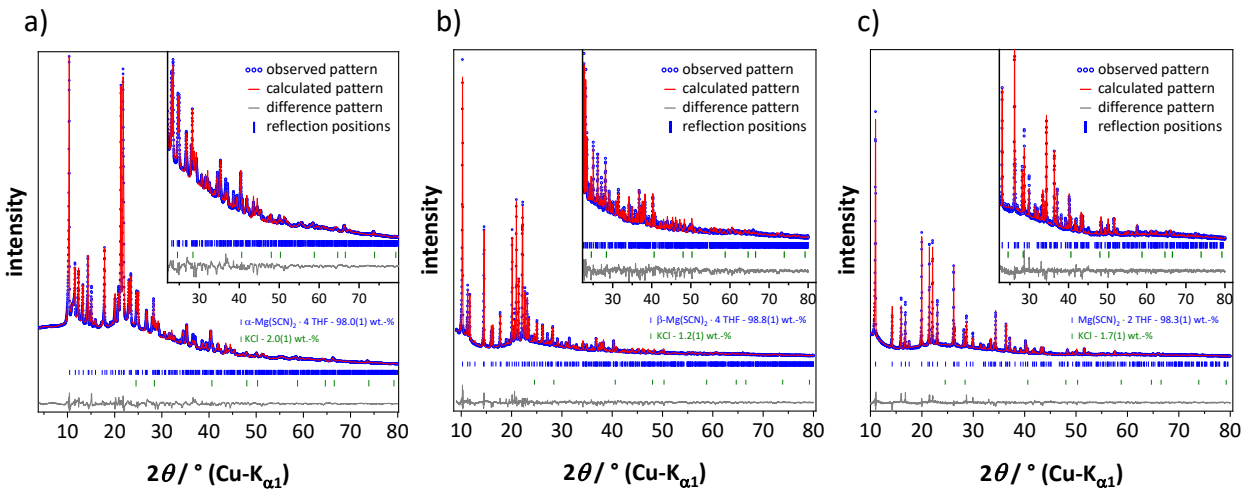

Figure S7: Final Rietveld refinement plots of the crystal structures of a) α-$Mg(SCN)_2 \cdot 4$ THF, b) β-$Mg(SCN)_2 \cdot 4$ THF and c) $Mg(SCN)_2 \cdot 2$ THF. The high 2θ regions are enlarged for clarity (inserts).

Table S7: Crystallographic and Rietveld refinement data of α-$Mg(SCN)_2 \cdot 4$ THF, β-$Mg(SCN)_2 \cdot 4$ THF and $Mg(SCN)_2 \cdot 2$ THF.

compound name	α-$Mg(SCN)_2 \cdot 4$ THF	β-$Mg(SCN)_2 \cdot 4$ THF	$Mg(SCN)_2 \cdot 2$ THF
molecular formula	$4(C_4H_8O)\cdot Mg(SCN)_2$	$4(C_4H_8O)\cdot Mg(SCN)_2$	$2(C_4H_8O)\cdot Mg(SCN)_2$
sum formula	$C_{18}H_{32}MgN_2O_4S_2$	$C_{18}H_{32}MgN_2O_4S_2$	$C_{10}H_{16}MgN_2O_2S_2$
molecular weight/ g/mol	428.871	428.871	284.685
temperature/ K	298	433	448
space group	$P2_1/n$ (no. 14)	$P2_1/a$ (no. 14)	$C2/m$ (no. 12)
Z	2	2	2
a /Å	15.2137(8)	10.5624(4)	10.9189(3)
b /Å	10.2054(4)	15.0999(5)	12.4373(4)
c /Å	7.7220(3)	7.8918(3)	5.7363(2)
β /°	94.980(2)	96.578(2)	105.144(2)
V /Å³	1194.39(9)	1250.37(7)	751.94(4)
ρ_{calc}/ g · cm^{-3}	1.19	1.14	1.26
wavelength / Å	1.5406	1.5406	1.5406
R-p /% [a)]	2.42	5.32	4.79
R-wp /% [a)]	3.22	6.41	6.44
R-F^2 /% [a)]	1.52	3.59	4.83
no. of variables	78	78	78

[a)]R-exp, R-p, R-wp and R-F² as defined in TOPAS (Bruker AXS).

Table S8: Atomic coordinates of α-$Mg(SCN)_2 \cdot 4$ THF, β-$Mg(SCN)_2 \cdot 4$ THF and $Mg(SCN)_2 \cdot 2$ THF.

Atom	Wyck.	Site	S.O.F.	x	y	z	B / Å²
α-$Mg(SCN)_2 \cdot 4$ THF, *T* = 298 K							
Mg(1)	2c	-1	1	1/2	0	1/2	3.0(3)[b]
C(1)	4e	1	1	0.0893(12)	0.321(2)	0.744(2)	3.0(3)[b]
N(1)	4e	1	1	0.0449(9)	0.389(2)	0.818(2)	3.0(3)[b]
S(1)	4e	1	1	0.1526(15)	0.224(2)	0.639(3)	3.0(3)[b]
O(11)	4e	1	1	0.6321(6)	0.973(2)	0.622(2)	3.0(3)[b]
C(11)	4e	1	1	0.6610(15)	0.881(2)	0.761(2)	3.0(3)[b]
C(12)	4e	1	1	0.6915(16)	1.086(2)	0.637(4)	3.0(3)[b]
C(13)	4e	1	1	0.7660(18)	1.049(5)	0.767(6)	3.0(3)[b]
C(14)	4e	1	1	0.732(2)	0.948(4)	0.873(4)	3.0(3)[b]
O(21a)	4e	1	0.64(1)	0.9637(6)	0.340(1)	0.170(3)	3.0(3)[b]
C(21a)	4e	1	0.64(1)	0.9049(7)	0.308(1)	0.304(2)	3.0(3)[b]
C(22a)	4e	1	0.64(1)	0.9981(11)	0.217(2)	0.106(3)	3.0(3)[b]
C(23a)	4e	1	0.64(1)	0.947(2)	0.109(2)	0.181(5)	3.0(3)[b]
C(24a)	4e	1	0.64(1)	0.9134(19)	0.163(2)	0.335(4)	3.0(3)[b]
O(21b)	4e	1	0.36(1)	0.9637(6)	0.340(1)	0.170(3)	3.0(3)[b]
C(21b)	4e	1	0.36(1)	0.996(2)	0.285(3)	0.339(3)	3.0(3)[b]
C(22b)	4e	1	0.36(1)	0.9347(18)	0.230(3)	0.056(4)	3.0(3)[b]
C(23b)	4e	1	0.36(1)	0.935(4)	0.111(2)	0.169(8)	3.0(3)[b]
C(24b)	4e	1	0.36(1)	0.996(4)	0.139(3)	0.317(6)	3.0(3)[b]
β-$Mg(SCN)_2 \cdot 4$ THF, *T* = 433 K							
Mg(1)	2a	-1	1	1/2	1/2	0	3.0(3)[b]
C(1)	4e	1	1	0.168(2)	0.903(2)	0.768(2)	3.0(3)[b]
N(1)	4e	1	1	0.095(2)	0.942(1)	0.839(2)	3.0(3)[b]
S(1)	4e	1	1	0.271(2)	0.848(2)	0.668(3)	3.0(3)[b]
O(11a)	4e	1	0.43(5)	0.486(2)	0.620(1)	0.150(2)	3.0(3)[b]
C(11a)	4e	1	0.43(5)	0.568(7)	0.690(3)	0.092(9)	3.0(3)[b]
C(12a)	4e	1	0.43(5)	0.402(4)	0.662(4)	0.263(6)	3.0(3)[b]
C(13a)	4e	1	0.43(5)	0.422(11)	0.759(3)	0.251(14)	3.0(3)[b]
C(14a)	4e	1	0.43(5)	0.535(13)	0.773(3)	0.179(16)	3.0(3)[b]
O(11b)	4e	1	0.57(5)	0.486(2)	0.620(1)	0.150(2)	3.0(3)[b]
C(11b)	4e	1	0.57(5)	0.482(12)	0.700(2)	0.042(5)	3.0(3)[b]
C(12b)	4e	1	0.57(5)	0.489(4)	0.649(4)	0.327(3)	3.0(3)[b]
C(13b)	4e	1	0.57(5)	0.466(14)	0.747(4)	0.322(11)	3.0(3)[b]
C(14b)	4e	1	0.57(5)	0.49(2)	0.777(2)	0.161(10)	3.0(3)[b]
O(21a)	4e	1	0.39(2)	0.652(2)	0.472(1)	0.183(2)	3.0(3)[b]
C(21a)	4e	1	0.39(2)	0.723(4)	0.502(4)	0.343(5)	3.0(3)[b]
C(22a)	4e	1	0.39(2)	0.741(5)	0.422(3)	0.089(6)	3.0(3)[b]
C(23a)	4e	1	0.39(2)	0.861(5)	0.411(7)	0.208(12)	3.0(3)[b]
C(24a)	4e	1	0.39(2)	0.857(4)	0.472(8)	0.341(10)	3.0(3)[b]
O(21b)	4e	1	0.61(2)	0.652(2)	0.472(1)	0.183(2)	3.0(3)[b]
C(21b)	4e	1	0.61(2)	0.687(4)	0.413(3)	0.327(4)	3.0(3)[b]
C(22b)	4e	1	0.61(2)	0.770(3)	0.505(3)	0.123(6)	3.0(3)[b]
C(23b)	4e	1	0.61(2)	0.877(3)	0.453(6)	0.218(12)	3.0(3)[b]
C(24b)	4e	1	0.61(2)	0.830(4)	0.413(6)	0.357(10)	3.0(3)[b]
$Mg(SCN)_2 \cdot 2$ THF, *T* = 448 K							
Mg(1)	2b	2/*m*	1	0	1/2	0	4.0(3)[b]
C(1)	8j	1	0.5	0.157(2)	0.515(1)	0.604(4)	4.0(3)[b]
N(1)	4i	m	1	0.117(1)	1/2	0.769(2)	4.0(3)[b]
S(1)	8j	1	0.5	0.213(2)	0.535(2)	0.369(4)	4.0(3)[b]
O(11a)	4g	2	0.601(6)	1/2	0.171(1)	0	4.0(3)[b]

C(11a)	8j	1	0.301(6)	0.516(8)	0.239(4)	0.215(6)	4.0(3)[b)]
C(12a)	8j	1	0.301(6)	0.509(7)	0.240(4)	-0.201(8)	4.0(3)[b)]
C(13a)	8j	1	0.301(6)	0.560(20)	0.346(7)	-0.090(20)	4.0(3)[b)]
C(14a)	8j	1	0.301(6)	0.510(30)	0.352(4)	0.128(19)	4.0(3)[b)]
O(11b)	4g	2	0.399(6)	1/2	0.171(1)	0	4.0(3)[b)]
C(11b)	8j	1	0.199(6)	0.613(4)	0.228(5)	-0.027(13)	4.0(3)[b)]
C(12b)	8j	1	0.199(6)	0.396(4)	0.249(4)	-0.041(16)	4.0(3)[b)]
C(13b)	8j	1	0.199(6)	0.440(13)	0.347(7)	-0.140(40)	4.0(3)[b)]
C(14b)	8j	1	0.199(6)	0.582(12)	0.345(4)	-0.030(40)	4.0(3)[b)]

[b)]one global parameter for the Beq of all sites was defined.

Table S9: Selected bond distances and angles in α-$Mg(SCN)_2 \cdot 4$ THF, β-$Mg(SCN)_2 \cdot 4$ THF and $Mg(SCN)_2 \cdot 2$ THF.

Atoms	Distance / Å	Atoms	Angle / °
α-$Mg(SCN)_2 \cdot 4$ THF, T = 298 K			
Mg(1)-O(11)	2x 2.163(9)	O(11)-Mg(1)-O(21)	83.8(4), 96.2(4)
Mg(1)-O(21)	2x 2.198(10)	O(11)-Mg(1)-N(1)	88.9(4), 91.1(4)
Mg(1)-N(1)	2x 1.978(13)	O(21)-Mg(1)-N(1)	83.3(5), 96.7(5)
β-$Mg(SCN)_2 \cdot 4$ THF, T = 433 K			
Mg(1)-O(11)	2x 2.183(13)	O(11)-Mg(1)-O(21)	83.4(6), 96.6(6)
Mg(1)-O(21)	2x 2.078(15)	O(11)-Mg(1)-N(1)	87.1(6), 92.9(6)
Mg(1)-N(1)	2x 1.925(15)	O(21)-Mg(1)-N(1)	82.6(7), 97.4(7)
$Mg(SCN)_2 \cdot 2$ THF, T = 448 K			
Mg(1)-O(11)	2x 2.126(9)	O(11)-Mg(1)-N(1)	2x 90
Mg(1)-N(1)	2x 2.069(11)	O(11)-Mg(1)-S(1)	2x 80.8(6), 99.2(6)
Mg(1)-S(1)	4x 2.741(19)	N(1)-Mg(1)-S(1)	2x 87.2(5), 92.8(5)

Thermal Decomposition

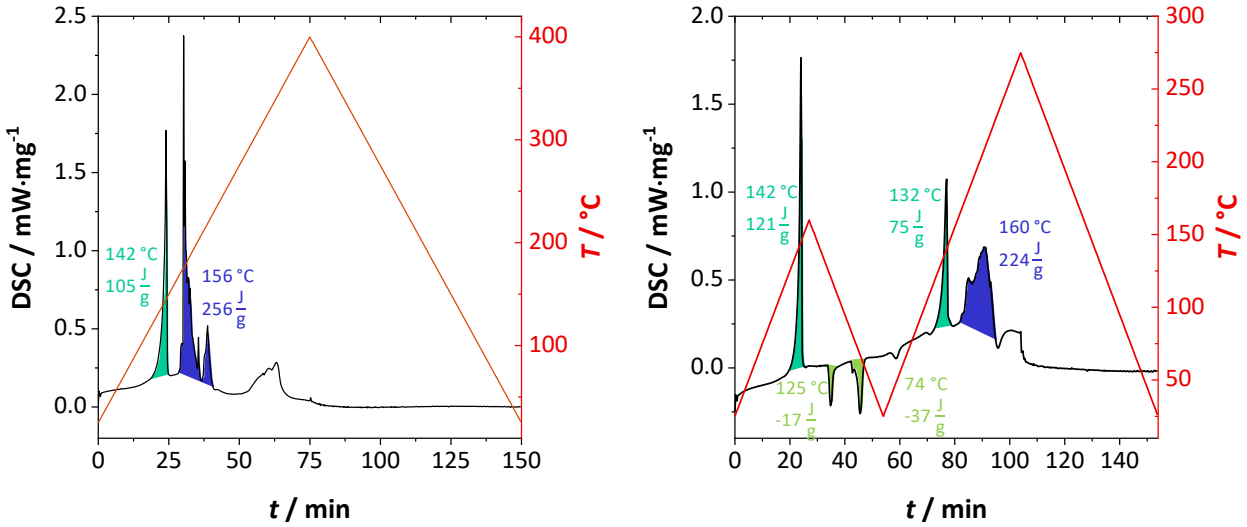

Figure S8: DSC measurements of $Mg(SCN)_2 \cdot 2\ H_2O \cdot 2$ THF with different heating programs.

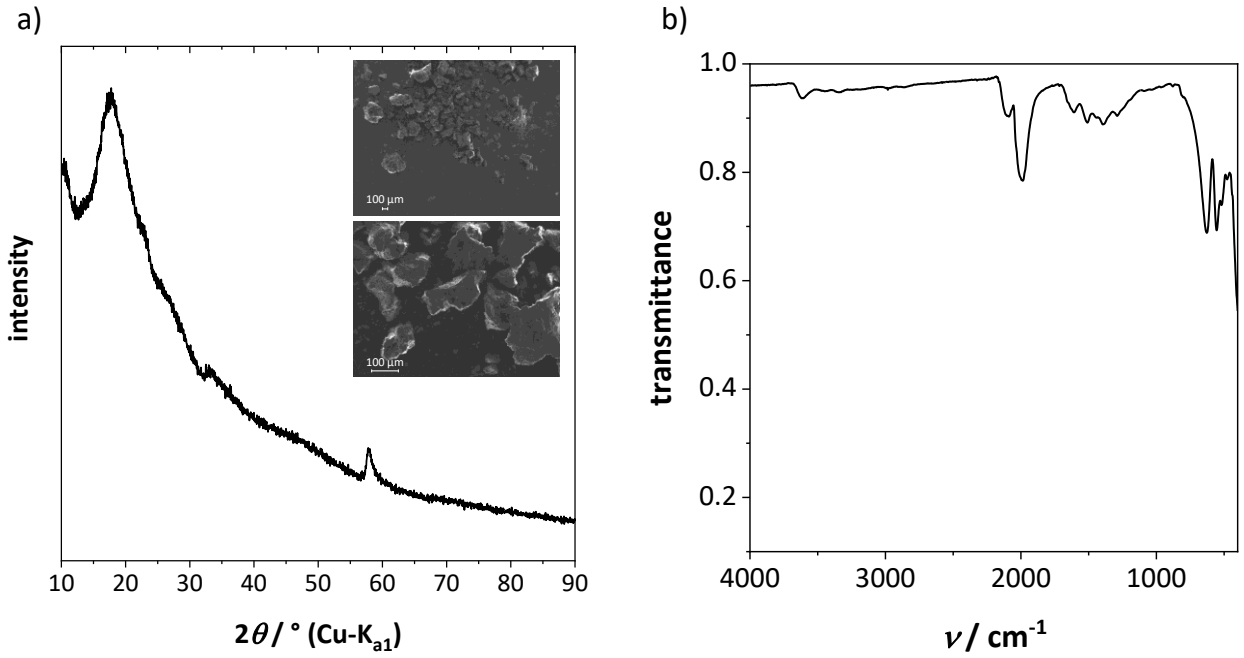

Figure S9: Thermal decomposition of $Mg(SCN)_2 \cdot 4\ H_2O$ after 400 °C heating in Ar inert-gas atmosphere. a) XRPD pattern with inserted SEM images; b) IR spectrum.

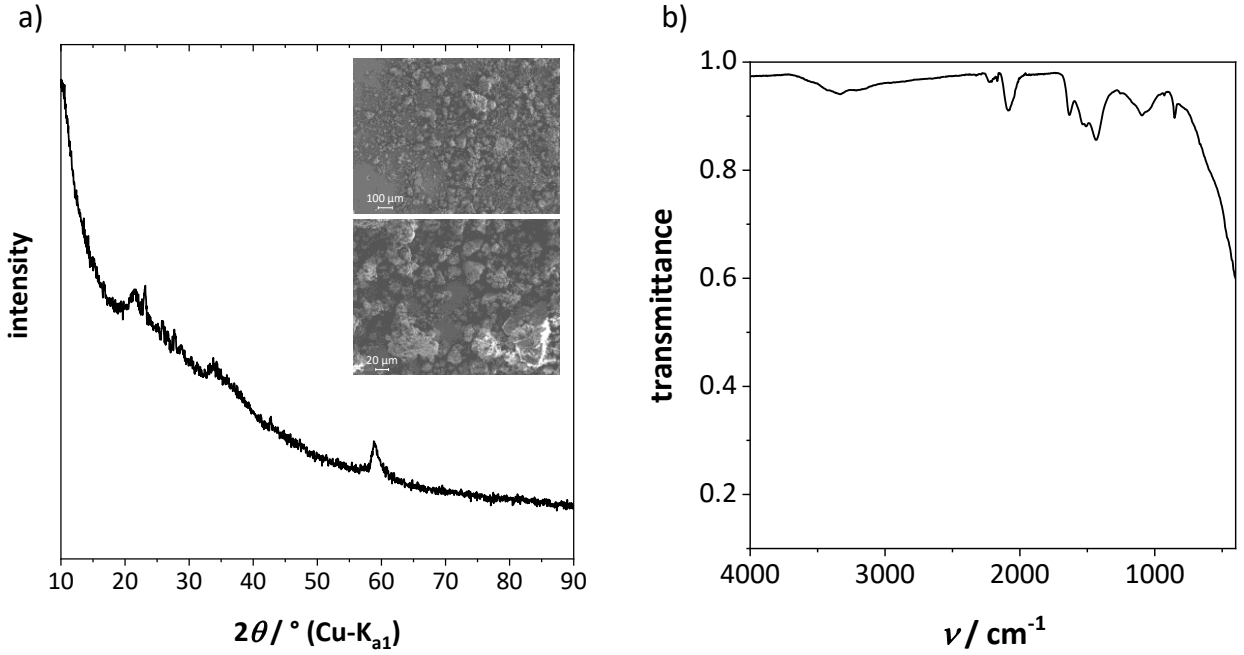

Figure S10: Thermal decomposition of $Mg(SCN)_2 \cdot 4$ THF after 400 °C heating in N_2 inert-gas atmosphere. a) XRPD pattern with inserted SEM images; b) IR spectrum.

Structure Description

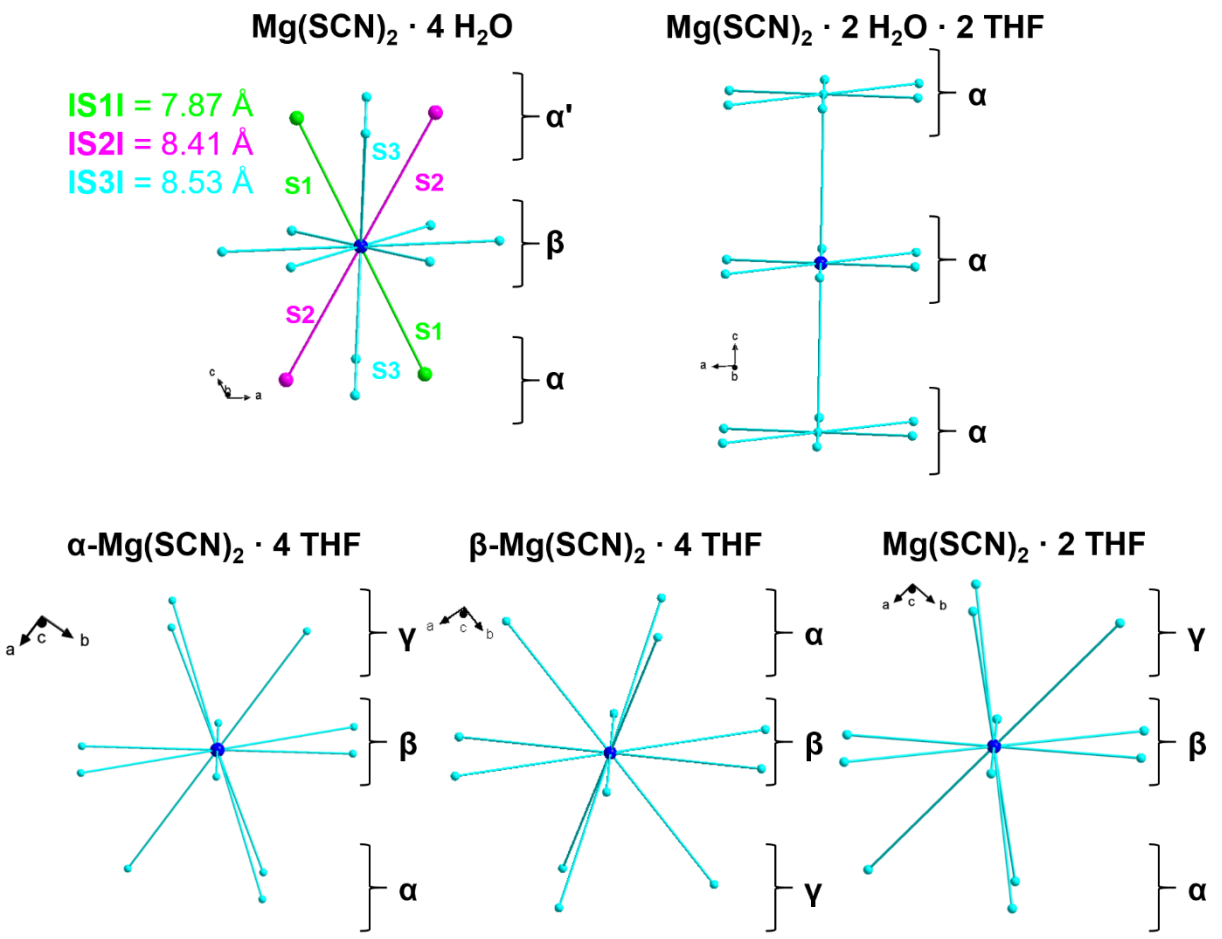

Figure S 11: Packing diagrams of the cation substructures of the investigated magnesium thiocyanate phases used for derivation of the stacking orders. Therefore, one magnesium cation (blue atom) was connected with its 12 ±v 2 nearest neighbours (cyan atoms and bonds). The cation positions are indicated by small Greek letters. Green and magenta toms and bonds indicate possible stacking vectors (S1, S2, S3) in the structure of $Mg(SCN)_2 \cdot 4\ H_2O$.

Lattice Expansion

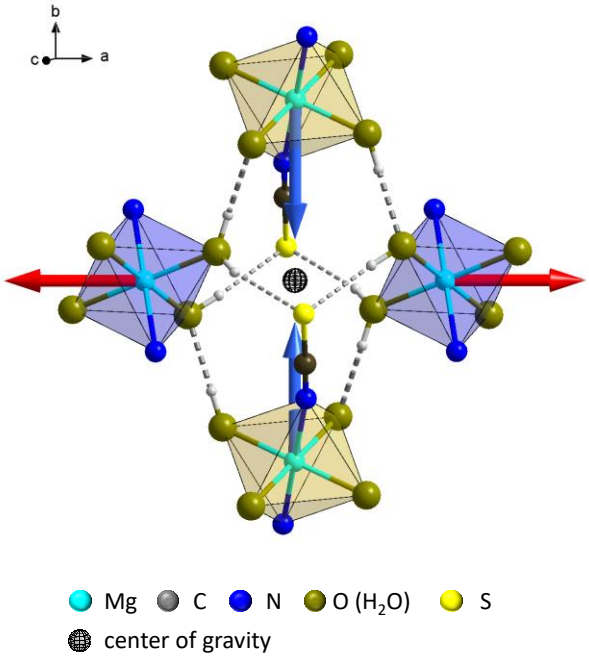

Figure S12: Excerpt of a layer in the crystal structure of $Mg(SCN)_2 \cdot 4\ H_2O$. H-bonds are indicated by dashed and dotted grey bonds, blue and red arrows indicate negative and positive thermal expansion.

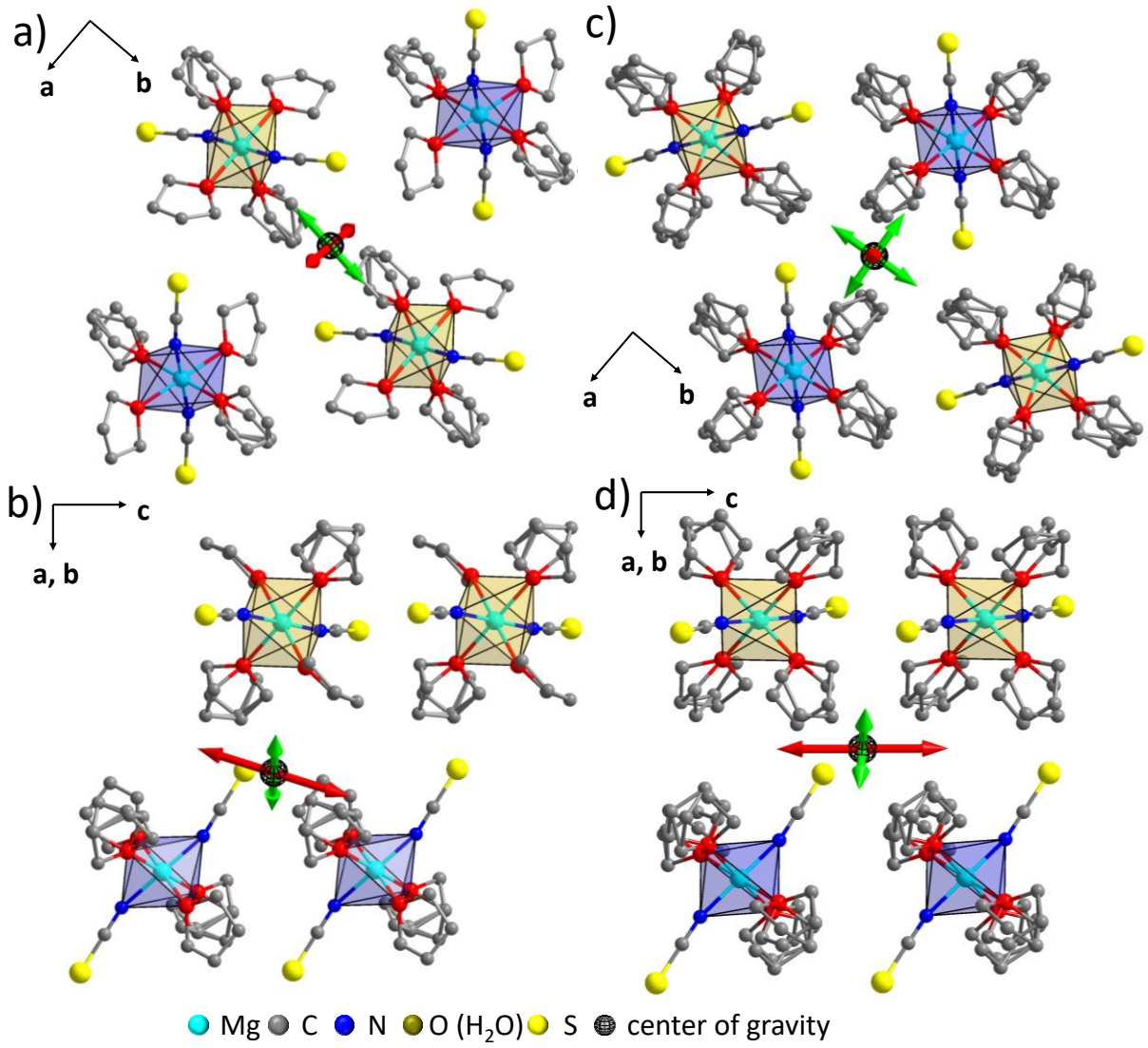

Figure S13: Excerpt of the packing diagrams of $Mg(SCN)_2 \cdot 4$ THF; a) and b) α-form, c) and d) β-form. Red arrows indicate strong and green arrows indicate medium positive thermal expansion along the principal axes (Table S10).

Table S10: Volume expansion coefficients V_α and all axes expansion coefficients of $Mg(SCN)_2 \cdot 4\ H_2O$, α-$Mg(SCN)_2 \cdot 4$ THF, β-$Mg(SCN)_2 \cdot 4$ THF and $Mg(SCN)_2 \cdot 2$ THF. α is the linear coefficient of the thermal expansion with $\sigma(\alpha)$ being the corresponding estimated standard deviation. *a*, *b* and *c* are the projections of the principal directions X_n (n = 1, 2 and 3) on the unit cell axes. Plots of the thermal expansion along the principal axes and of the overall volume expansion are given in Figure S14.

axes	α / 10^{-6} K^{-1}	$\sigma(\alpha)$ / 10^{-6} K^{-1}	a	b	c
$Mg(SCN)_2 \cdot 4\ H_2O$					
X_1	-44.0	2.0	0	-1	0
X_2	31.5	0.5	-0.3224	0	-0.9466
X_3	165.4	4.1	0.9965	0	0.0839
V_α	152.9	1.8			
α-$Mg(SCN)_2 \cdot 4$ THF					
X_1	3.3	1.1	-0.8050	0	0.5933
X_2	90.0	0.6	0	1	0
X_3	172.7	0.5	0.2209	0	0.9753
V_α	268.0	1.8			
β-$Mg(SCN)_2 \cdot 4$ THF					
X_1	37.9	1.0	-1	0	-0.0082
X_2	49.6	0.9	0	1	0
X_3	128.4	2.9	0.0808	0	0.9967
V_α	216.5	2.8			
$Mg(SCN)_2 \cdot 2$ THF					
X_1	-15.8	0.5	-0.0409	0	0.9992
X_2	36.2	1.5	0	1	0
X_3	219.4	2.3	-0.8451	0	-0.5346
V_α	240.5	3.7			

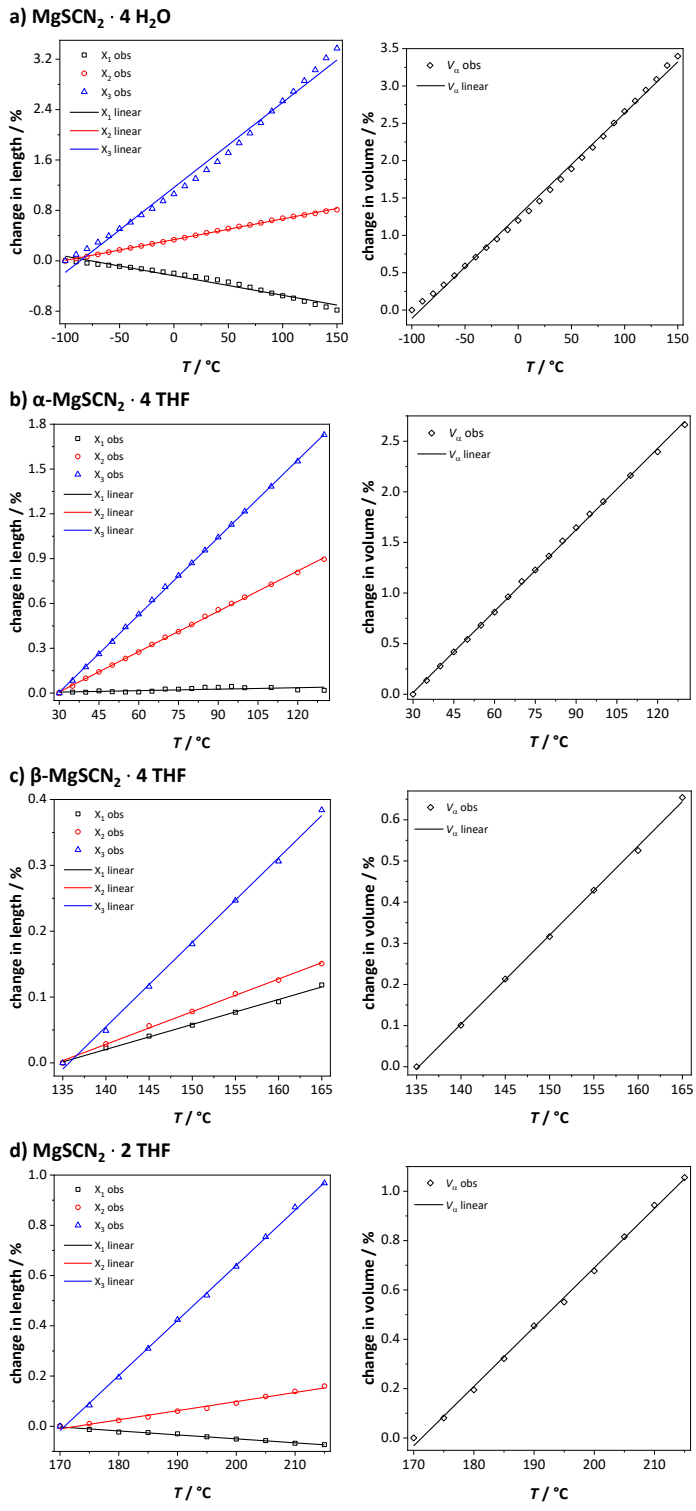

Figure S14: Plots of the thermal expansion along the principal axes and of the overall volume expansion of a) $Mg(SCN)_2 \cdot 4\ H_2O$, b) α-$Mg(SCN)_2 \cdot 4$ THF, c) β-$Mg(SCN)_2 \cdot 4$ THF and d) $Mg(SCN)_2 \cdot 2$ THF.

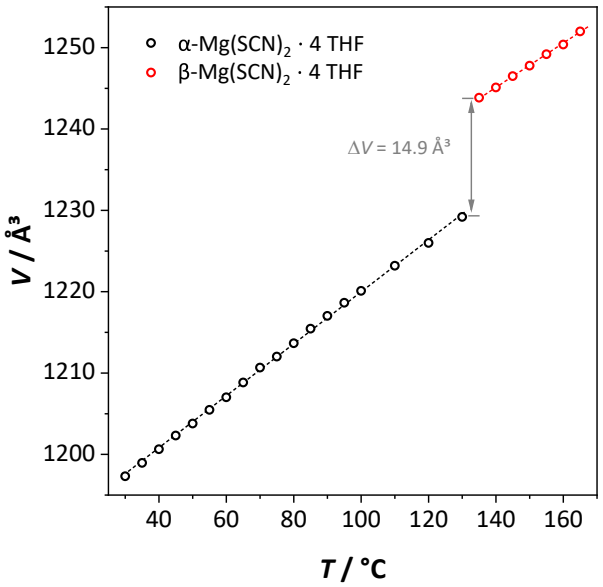

Figure S15: Evolution of the unit cell volume of α-$Mg(SCN)_2 \cdot 4$ THF during heating including the discontinuous volume expansion (grey arrow) associated with the transition into the β-form.

References

1 S. C. Mojumdar, M. Melník, E. Jóna and D. Hudecová, *Chem. Pap.*, 1999, **53**, 265–271.
2 A. A. Coelho, *J. Appl. Crystallogr.*, 2018, **51**, 210–218.
3 H. M. Rietveld, *J. Appl. Crystallogr.*, 1969, **2**, 65–71.
4 K. Mereiter and A. Preisinger, *Acta Crystallogr.*, 1982, **B38**, 1263–1265.
5 S. Bette, G. Eggert, S. Emmerling, M. Etter, T. Schleid and R. E. Dinnebier, *Cryst. Growth Des.*, 2020, **20**, 5346–5355.
6 M. J. Cliffe and A. L. Goodwin, *J. Appl. Crystallogr.*, 2012, **45**, 1321–1329.
7 A. A. Coelho, *J. Appl. Crystallogr.*, 2003, **36**, 86–95.
8 J. L. F. A. Le Bail , H. Duroy, *Mater. Res. Bull.*, 1988, **23**, 447–452.
9 R. W. Cheary and A. Coelho, *J. Appl. Crystallogr.*, 1992, **25**, 109–121.
10 R. W. Cheary, A. A. Coelho and J. P. Cline, *J. Res. Natl. Inst. Stand. Technol.*, 2004, **109**, 1–25.
11 H. Ott, *Z. Kristallogr.*, 1926, **63**, 222–30.
12 A. A. Coelho, *J. Appl. Crystallogr.*, 2000, **33**, 899–908.
13 E. Dubler, A. Reller and H. R. Oswald, *Z. Kristallogr.*, 1982, **161**, 265–277.
14 V. Favre-Nicolin and R. Černý, *Mater. Sci. Forum*, 2004, **443–444**, 35–38.
15 G. Oszlányi and A. Süťo, *Acta Crystallogr.*, 2004, **A60**, 134–141.
16 C. Baerlocher, L. B. McCusker and L. Palatinus, *Z. Kristallogr.*, 2007, **222**, 47–53.
17 A. A. Coelho, *Acta Crystallogr.*, 2007, **A63**, 400–406.